Direct Bottom-Up Synthesis of $ZnAl_2O_4$ Nanoparticle via Organic Ligand Dissolution Method

Takayuki Nakane[1], Takashi Naka[2], Minako Nakayama[2] and Tetsuo Uchikoshi[1]

1. National Institute for Materials Science, Research Center for Electronic and Optical Materials, 1-2-1, Sengen, Tsukuba, 305-0047 Ibaraki, Japan
2. National Institute for Materials Science, Research Center for Materials Nanoarchitectonics (MANA), 1-1, Namiki, Tsukuba, 305-0044 Ibaraki, Japan

Corresponding Author: Takayuki Nakane NAKANE.Takayuki@nims.go.jp

Abstract

This study improves the hydrothermal synthesis of $ZnAl_2O_4$ to realize direct bottom-up chemical synthesis from a liquid precursor solution. The liquid solution was prepared by the organic ligand dissolution (OLD) method. Synthesized $ZnAl_2O_4$ was identified as a single phase comprising $ZnAl_2O_4$ with organic components speculated to work as surfactants that aid in size stabilization. The synthesized $ZnAl_2O_4$ product was observed to be in nanoparticle form, exhibiting a wide-bandgap attribute to the quantum size effect. The growth rate of $ZnAl_2O_4$ nanoparticles in the proposed method is low, and a series of results revealed the phase formation process of synthesized $ZnAl_2O_4$. This formation process seems common for chemically synthesized $ZnAl_2O_4$ and indicates the importance of compositional analysis in the study for chemical synthesis of this material. The application of the OLD method enables us to synthesize $ZnAl_2O_4$ across a wide pH range (3 ~ 11), and it is applicable to the continuous synthesis using a flow-type reaction system of hydrothermal reaction. Moreover, our technique is basically applicable to the synthesis of other spinel oxide. These characteristics of the OLD method are expected to extensively improve the investigation of chemical processing of spinel oxides.

Keywords Hydrothermal Synthesis, Chemical Synthesis, Nanoparticle, $ZnAl_2O_4$, Spinel

Introduction

$ZnAl_2O_4$ is an important spinel oxide. This material consists of ubiquitous, inexpensive, and nontoxic elements that have low environmental loads, and it shows excellent chemical and thermal stability. From the viewpoint of the electric structure, a wide band-gap of over 3.8 eV gives some attractive characteristics [1,2]. Thus, this material is being actively investigated for its optical properties [3-5], its application to sensing devices [6,7], and its catalytic performance [8-10]. In particular, the surface state of this material is similar to that of ZnO or γ-Al_2O_3, hence this material itself also shows an excellent catalytic properties. For instance, the photocatalytic properties of $ZnAl_2O_4$ have been utilized for the decomposition of dye [8,11-13] or some pollutants [14,15]. The catalytic performance of $ZnAl_2O_4$ has also been reported in various applications, including the decomposition of the steam during the ethanol reforming [9], the combustion of soot in a NO_2/O_2 atmosphere [10], and the combustion of iso-butane [11].

These pioneering reports for $ZnAl_2O_4$ stimulated us to further investigate its potential for industrial application. From this viewpoint, the development of a chemical processing technique for $ZnAl_2O_4$ is an important issue, since the cost of production will be a key in its utilization. In general, the synthesis temperatures of aluminum compounds are relatively high, because aluminum and/or oxides require high energy to react with the other materials. This is one reason why it is difficult to establish a chemical synthesis technique for $ZnAl_2O_4$. Chemical synthesis of $ZnAl_2O_4$ is generally conducted by a technique based on the sol-gel method [9,13-18] or the Pechini method [19]. The former chemically prepares a

layered-double-hydroxide (LDH) precursor involving Zn^{2+} and Al^{3+} by mixing these salts in solution. The later dissolves Zn^{2+} and Al^{3+} salts in water separately, and the resulting solutions are mixed [7]. These chemical synthesis techniques relatively reduces the heating temperature compared to that in the solid-state reaction and help to improve the homogeneity of the product. However, almost all techniques use water-insoluble precipitants or suspensions as precursors [7-22], and thus we cannot expect size homogeneity based on the bottom-up creation of nano crystalline. Moreover, these chemically prepared precursors often require after-sintering in the furnace, similar to a solid-state reaction, and the temperature is higher than 500 ^{o}C [7-14,17,18,21]. This kind of synthesis route was improved recently by the application of microwave heating techniques [11,20,21]. These techniques do not require heating to such high temperature, but they still require water-insoluble precursors.

Water-insoluble precursors are not convenient, however, especially in industrial applications entailing mass synthesis. Thus, a direct bottom-up synthesis technique from a liquid precursor solution is desired for the fabrication of $ZnAl_2O_4$. In addition, a chemical synthesis technique for ceramic oxides like $ZnAl_2O_4$ commonly requires alkaline solution, because oxide produced from acidic solution often involves numerous deficiencies. Therefore, preparing a liquid precursor solution that can be used in alkaline region is considered a meaningful challenge for promoting the industrial application of $ZnAl_2O_4$.

Both Zn and Al contain some water-soluble compounds, but their coexistence in alkaline solution is not easy to achieve. Both Zn and Al are known as amphoteric elements, but they can solve as metal ions in

acidic solution and as complex ions in alkaline one. This difference decreases the solubility of these ions in the neutral pH region. In fact, water-soluble compounds of Zn^{2+} and Al^{3+} basically decrease the pH when they are solved in water. However, pH tuning of the solution from the acidic to the alkaline one is quite difficult and yields a lot of precipitation of hydroxides. Hence, almost all studies for the chemical synthesis of $ZnAl_2O_4$ used precipitant such as LDH, which is obtained in alkaline solution, as a precursor [7-22]. To address this worrisome issue, we were inspired to use organic acid salt. The addition of organic acid salt decreases the pH of water, thus the solubility of Zn^{2+} and that of Al^{3+} are speculated to be high in this solution. Even so, we can expect that both Zn^{2+} and Al^{3+} dissolve in this solution as complex ions with ligands originated in the organic acid. These complex ions are expected to be stable in alkaline solution even though the pH of the solution is increased by adding some bases. That is, the addition of organic acid salt to a solution of Zn^{2+} and Al^{3+} is considered to provide a liquid precursor solution usable across a wide pH range.

Based on this concept, we here successfully synthesized $ZnAl_2O_4$ by applying a hydrothermal technique using a liquid precursor solution of organic acid with Zn^{2+} and Al^{3+} salts. This preparing technique of a liquid precursor solution is named as organic-ligand dissolution (OLD) method. This technique is basically applicable to the synthesis of other spinel oxides. Therefore, we believe that the OLD method can extensively contribute to the investigations into the application for chemical processing of the spinel oxides.

Experimental

$ZnAl_2O_4$ samples were synthesized in nanoparticle form by applying a hydrothermal technique using a liquid precursor solution. First, $Zn(CH_3COO)_2 \cdot 2H_2O$ (99.9 %: FUJIFILM Wako Pure Chemical: Japan), $Al_2O(CH_3COO)_3 \cdot nH_2O$ (14.8 ~ 18.0 % as Al: Kanto Chemical: Japan) and citric acid (98.0 %: FUJIFILM Wako Pure Chemical: Japan) as the organic components of the OLD method were dissolved in distilled water and mixed for over 3 days. This long mixing process made a liquid precursor solution from the translucent to the transparent. The mixing ratio was w : 1 : 2 of $Zn(CH_3COO)_2 \cdot 6H_2O$, $Al_2O(CH_3COO)_3 \cdot nH_2O$ and citric acid with the concentration of the expected product ($Zn_wAl_2O_4$) controlled at 0.05 M. Second, the pH of this transparent precursor solution was adjusted by adding ammonia solution (28%: Kanto Chemical, Japan), and its value was checked by using pH indicators (MN92118, MN92120 and MN92125: Macherey-Nagel: Germany). The amount of ammonia solution was controlled in the range of 0 ~ 4 ml as appropriate. Third, hydrothermal synthesis was performed for this pH-tuned precursor solution in a PTFE vessel including 15% carbon fiber (HUTc-25: SAN-AI Kagaku, Japan) enclosed in a stainless steel container (HU-25: SAN-AI Kagaku: Japan). This container was set in a furnace at a constant heating temperature in the range of 200 ~ 260 °C, and the pressure in the PTFE vessel was controlled to 10 MPa. The container was quenched in a water bath after hydrothermal synthesis for 2 ~ 24 hours. Fourth, synthesized $ZnAl_2O_4$ nanoparticles in the vessel were refined in the solution with 1ml of H_2SO_4 and 40 ml

of distilled water twice to remove excess ZnO impurity by a combination of centrifugation and decantation. Fifth, the refined nanoparticles were washed in distilled water twice by the same procedure used above for refinement. The obtained product $ZnAl_2O_4$ nanoparticles were dried under vacuum. As a reference, this study used $ZnAl_2O_4$ powder fabricated by a solid-state reaction. The fabrication and the characterization procedure of this powder are described elsewhere [23].

The phase contents, lattice constants, and average crystalline sizes of these nanoparticles were examined using a powder X-ray diffractometer (XRD, mini-Flex: Rigaku: Japan). The crystalline sizes were estimated from the full width at half maximum (FWHM) of the diffraction peaks by employing the Scherer equation [24,25]. The composition of the product $ZnAl_2O_4$ nanoparticles was evaluated using an inductively coupled plasma optical emission spectrometer (ICP-OES, 720-ES ICP-OES: Agilent Technologies: USA). The carbon amount in the product $ZnAl_2O_4$ nanoparticles was measured by the combustion infrared absorption method (CS444-LC: LECO Japan: Japan). On the other hand, optical absorbance for each sample was measured using a powder diffuse reflectance ultraviolet-visible spectroscopy (UV-Vis, V-650: JASCO Global: Japan) to discuss the bandgap of the $ZnAl_2O_4$ nanoparticles and by using a fourier transform infrared spectroscopy (FT-IR, FT/IR-6200: JASCO Global: Japan) for the samples in KBr pellets to obtain information on the residual organic components in the sample. For discussing these optical spectra, UV-VIS and FT-IR spectra were converted into the absorption spectra using the Kubelka-Munk equation [26]. Additionally, we simulated UV-VIS spectra using CASTEP [27,28]

for further comparison. The crystal structural data of $ZnAl_2O_4$ for CASTEP were previously obtained for the reference sample by using synchrotron XRD and Rietveld analysis [23,29,30]. For the calculation, we used OTFG ultrasoft as the pseudopotential, a plane wave basis set with a cutoff energy of 571.4 eV, and 5×5×5 as the K-point set, and we performed a full cell optimization. On the other hand, the morphology of the $ZnAl_2O_4$ nanoparticles was observed by transmission electron microscopy (TEM, JEM-2000F: Japan Electron: Japan) with an accelerating voltage of 200 kV.

Results and Discussion

$ZnAl_2O_4$ nanoparticles were successfully fabricated by hydrothermal synthesis via the OLD method. Typical XRD patterns of $ZnAl_2O_4$ nanoparticle are shown in Figure 1. The figure compares the effect of the heating time for the precursor solution of w = 1.0 and pH = 10.5. The precursor solution was a transparent liquid without precipitants. That is, this figure demonstrates the success of our proposed synthesis route for $ZnAl_2O_4$ from a liquid precursor solution usable in the alkaline region. In this case, heating temperature is an important parameter for obtaining the $ZnAl_2O_4$ phase as the product, since the XRD pattern of the sample heated at 200 ^oC is assigned as boehmite. On the other hand, the FWHM of each XRD pattern implies that long duration of hydrothermal synthesis promotes the growth of the particle size. As the next step, the influence of the pH of the precursor solution (w = 1.0) on the product was verified by reducing the amount of ammonia solution. Figure 2 shows the results. The precursor solutions were all

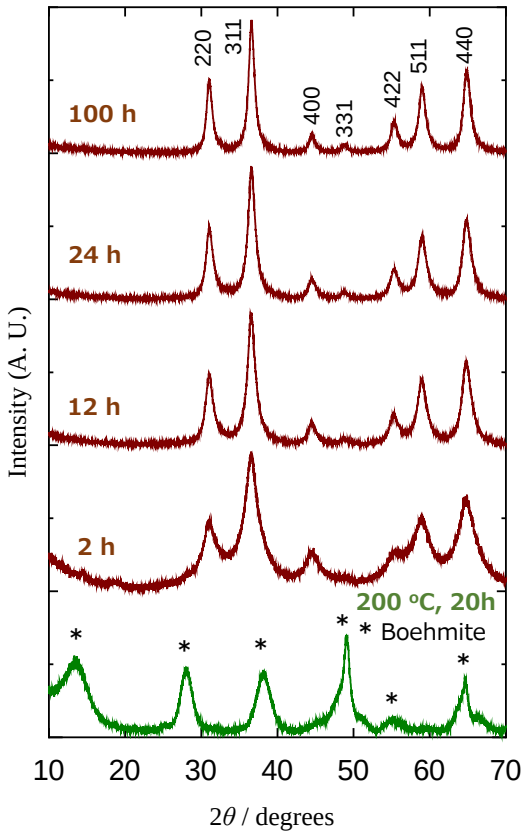

Fig. 1 Heating time dependence of the XRD patterns of $ZnAl_2O_4$ products synthesized at 260 °C in a hydrothermal atmosphere for the precursor of w = 1.00 and pH ≈ 10.5. For comparison, the bottom data in green line shows XRD pattern of the product heated at 200 °C for 20 hours.

transparent liquid without precipitants, indicating that liquid precursor solution of the OLD method is usable across a wide pH range (3.0 ~ 11). Interestingly, the XRD pattern of $ZnAl_2O_4$ shows sharp peaks in the case of the product from the precursor of pH = 11. These peaks seem to originate in the large particle size of $ZnAl_2O_4$, since excess ammonium water suppresses the citric acid working as the surfactant to the generated nanoparticles. Figure 3 focuses on the 440 peak of the XRD patterns plotted in Figure 2. We can find differences in FWHM between the products made from the acidic precursor (pH < 3.5), from the neutral one (5 < pH < 10), and from the alkaline one (pH > 10.5).

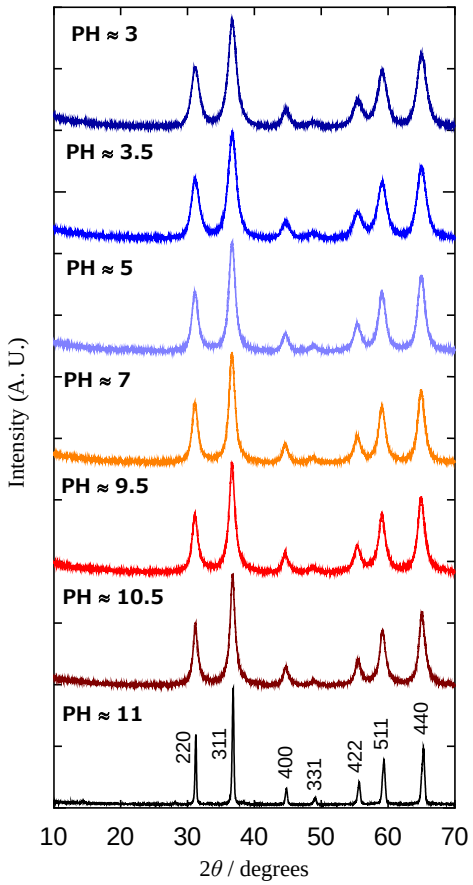

Fig. 2 **Influence of pH on the XRD pattern of product $ZnAl_2O_4$ nanoparticles made from precursor with w = 1.00. The hydrothermal synthesis conditions in all cases were 260 ºC for 24 hours.**

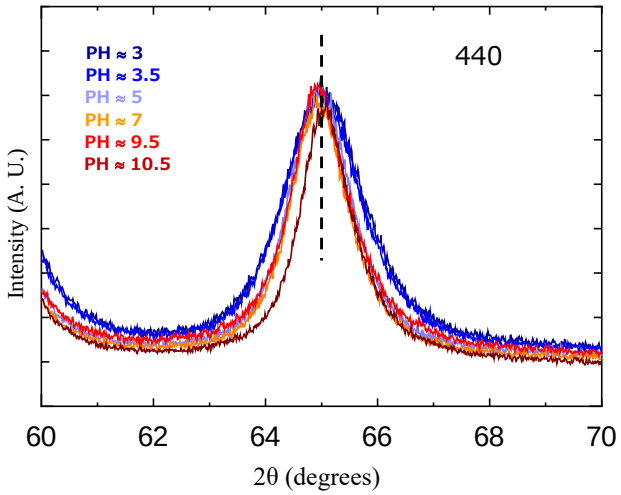

Fig. 3 **Comparison of the FWHM of the 440 peak in the XRD pattern of product $ZnAl_2O_4$ nanoparticles to reveal the influence of the precursor pH with w = 1.00. The hydrothermal synthesis conditions were all 260 ºC for 24 hours.**

Figure 4 (a) plots the carbon amounts of $ZnAl_2O_4$ nanoparticles shown in Figure 2 against the pH of the

precursor solution. This result is consistent with the speculation about citric acid working as the surfactant. Increasing the pH of the precursor solution indicates the sum titration of citric acid by ammonium water, so, it is considered to decrease the coupling activity as the surfactant. Thus, increasing the pH results in growth in both the size and surface area of $ZnAl_2O_4$ nanoparticles in the region of pH < 7. Probably, the coupling activity of citric acid as the surfactant saturates (or deteriorates) in the region of pH > 7, and the amount of the surfactant does not correspond to the increase in the surface area of $ZnAl_2O_4$ nanoparticles.

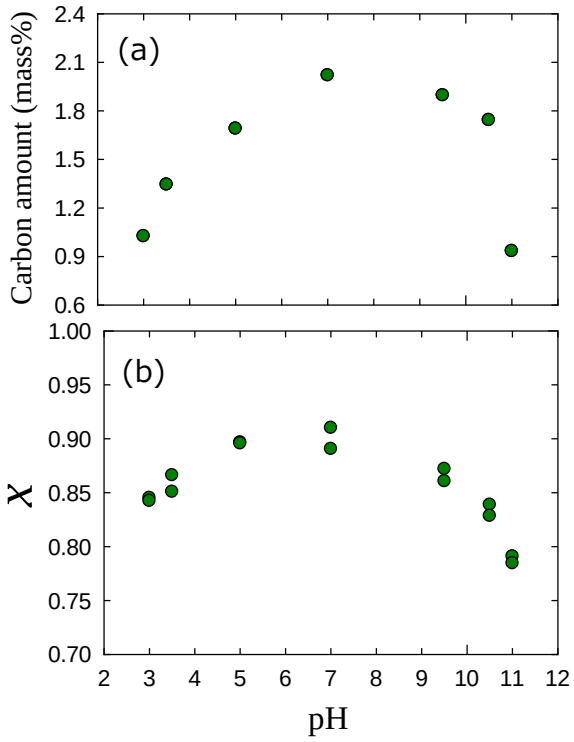

Fig. 4 **Dependence of (a) carbon amount and (b) relative Zn amount expressed as *x* against Al amount defined as 2 on pH of the precursor with *w* = 1.00 for the product $ZnAl_2O_4$ nanoparticles synthesized at 260 °C for 24 hours.**

Although the mechanism underlying this relationship between pH and the carbon amount in $ZnAl_2O_4$ nanoparticles remains to be clarified, above discussion implies that the pH of the liquid precursor solution

influences the quality of the product $ZnAl_2O_4$ nanoparticles. This point is further verified by the result of ICP-OES. Experimental data of ICP-OES indicate the change in the molar ratio of Zn and Al in $ZnAl_2O_4$ nanoparticles made from a precursor with different pH values. Here, the elemental ratios (i.e., Al/Zn) of all results were higher than 2 (i.e., they were Al-rich) even though the reference data measured for the $ZnAl_2O_4$ fabricated by a solid-state reaction shows reasonable value (i.e., ≈ 2). Considering the phase stability of the spinal structure and the charge valance of $ZnAl_2O_4$, it is difficult to imagine an extremely deficient composition such as $Zn_{0.5}Al_{1.15}O_{2.225}$. Consequently, we fix the Al content to 2.0 and calculate the x of $Zn_xAl_2O_{3+x/2}$ composition from the raw Al/Zn data obtained by ICP-OES measurement. Figure 4 (b) plots the x value against the pH of the precursor solution. Figures 4 (a) and (b) show similar curvatures. These results at least indicate the incompleteness of the product nanoparticle as $ZnAl_2O_4$ with respect to the chemical composition, and the neutral region of pH ≈ 7 seems to be the best for obtaining typical $ZnAl_2O_4$. Therefore, we verify the influence of the mixing process's w parameter, which defines the $Zn_wAl_2O_4$ composition in the precursor solution, on the x in the resulting product nanoparticle's $Zn_xAl_2O_{3+x/2}$ composition. Here, the pH of the precursor solution was fixed at pH ≈ 7. Figure 5 plots the variation of x in the nanoparticle made from the precursor solution at pH ≈ 7 with different compositions ($1.00 \leq w \leq 2.50$) and compares the impact of hydrothermal synthesis duration on the final product's x value. The figure indicates that hydrothermal synthesis using the precursor of the nominal initial composition (i.e., $w = 1.0$) tends to yield Zn-deficient $ZnAl_2O_4$ nanoparticles. Increasing the w value can modify this, but excess

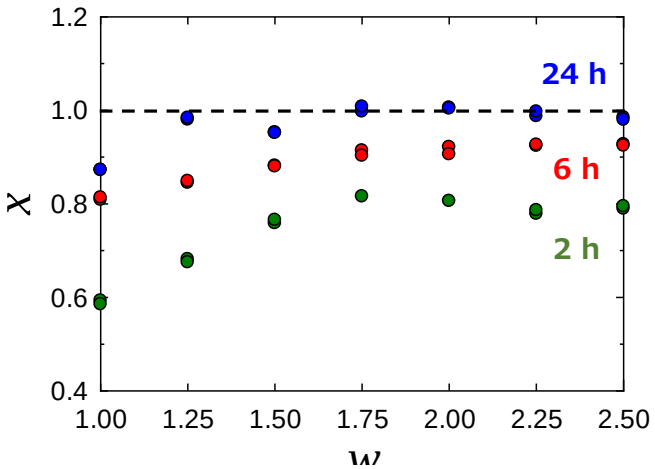

Fig. 5 **Relationship between the relative Zn amount (expressed as *x*) against the Al amount (defined as 2) in the prepared composition (expressed as *w*) of the product $ZnAl_2O_4$ nanoparticle. Hydrothermal synthesis was performed for the same precursor with *w* = 2.00 and pH ≈ 7, with heating at 250 °C. The results were differentiated and represented using different plotting colors to indicate the varying heating times. Green, red, and blue represent the product heated for 2, 6, and 24 hours, respectively.**

preparation ($w \geq 1.75$) does not promise to overcome the Zn deficiency. To control the chemical composition of the final product $ZnAl_2O_4$ nanoparticles, the important parameter is the duration of the hydrothermal synthesis rather than the *w* of the precursor solution. Figure 6 plots the *x* of the nanoparticles made from the precursor solution with pH ≈ 7 under different synthesis times. The result directly indicates the importance of the duration of hydrothermal synthesis via the OLD method; it should be longer than 1000 minutes (≈ 16.7 h) for obtaining $ZnAl_2O_4$ nanoparticles with the appropriate chemical composition. This means that $Zn_xAl_2O_{3+2/x}$ with a deficient Zn^{2+} is incorporated during the hydrothermal process. Then, Figure 1 shows that low-temperature synthesis yields boehmite as the product powder. Furthermore, our background experiments reveal that our synthesis condition cannot yield γ-Al_2O_3 (spinel structure) in the case of the precursor solution without Zn salt; i.e., the existence of Zn^{2+} in the precursor solution is

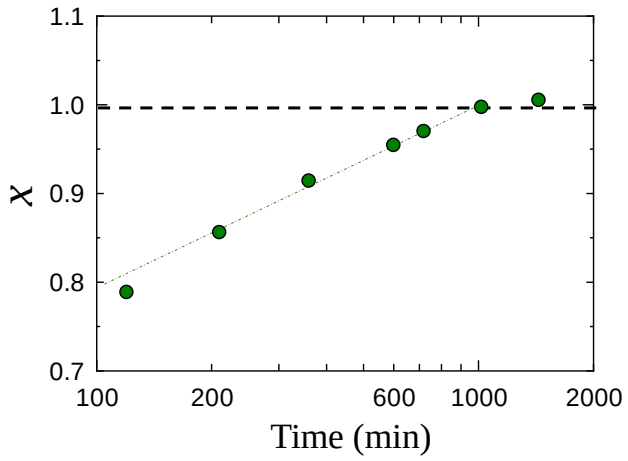

Fig. 6 Heating time dependence of the relative Zn amount expressed as *x* of the product $ZnAl_2O_4$ nanoparticle made from the precursor with *w* = 2.00 and pH ≈ 7. Hydrothermal synthesis was performed at 250 °C.

important for the formation of the spinel oxide under the condition of our hydrothermal synthesis. From these data, we speculated that the phase formation process of $ZnAl_2O_4$ nanoparticles by hydrothermal synthesis via the OLD method proceeds as follows.

$$\text{AlOOH (boehmite)} \rightarrow Zn_xAl_2O_{3+2/x} \text{ (deficient spinel)} \rightarrow ZnAl_2O_4$$

Of course, this speculation simplifies the compositional change, and the real process is thought to be more complicated. For instance, we should mind the possibility of (Zn,Al)OOH. A deficiency of Al^{3+} at each process has not yet been excluded as a possibility. In addition, we should also mind the occurrence of the site exchange phenomenon between Zn^{2+} and Al^{3+} in the case of the spinel aluminate composition. However, our speculation is essentially similar to the actual phase formation process of $ZnAl_2O_4$ nanoparticles during hydrothermal synthesis using the OLD method.

In the next step, we compared the UV-Vis spectra of our product $ZnAl_2O_4$ nanoparticles with those of a sintered reference sample. Additionally, we simulated $ZnAl_2O_4$ spectra using CASTEP [27,28] for further comparison. Figure 7 compares these three spectra. There are some differences between the spectra of the sintered reference sample and that of the simulation, but they are essentially similar. On the other hand, the spectra of our $ZnAl_2O_4$ nanoparticle looks quite different from the other spectra. Figure 8 shows TEM images of this sample. The $ZnAl_2O_4$ nanoparticles exhibited strong agglomeration, so that identification of each nanoparticle was difficult. However, we inferred from this figure that our $ZnAl_2O_4$ nanoparticle is a square-shaped nanocrystalline (see the dashed orange line) with an average particle size of about 4~8 nm (at least less than 10 nm). The particle size of this sample is calculated as 6.47 nm from the FWHM of the XRD pattern. This is consistent with the particles observed in Figure 8. A size of less than 10 nm is small

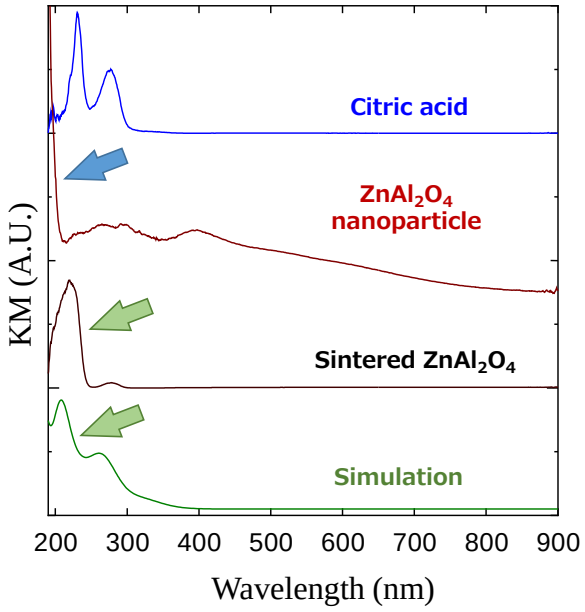

Fig. 7 UV-Vis spectrum of $ZnAl_2O_4$ nanoparticle synthesized at 250 °C for 20 hours from the precursor with w = 2.00 and pH ≈ 7. Data are compared with the UV-Vis spectrum of sintered $ZnAl_2O_4$ powder heated at 1300 °C as well as with the simulated results obtained by CASTEP and the spectrum of citric acid.

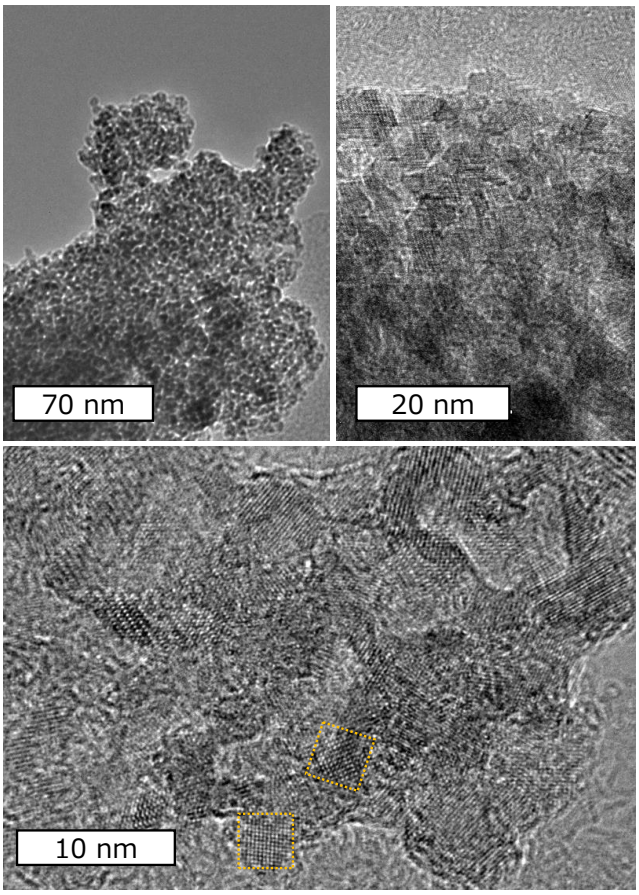

Fig. 8 TEM images of $ZnAl_2O_4$ nanoparticle synthesized at 250 °C for 20 hour from the precursor with w = 2.00 and pH ≈ 7.

enough to induce the quantum size effect. Therefore, UV-Vis spectrum is considered to shift to a higher energy region in the case of $ZnAl_2O_4$ nanoparticles than in the case of the sintered sample. We speculated that the origin of the peak indicated by the blue arrow in Figure 7 is the same as that of the peak indicated by the green arrow. On the other hand, the broad absorption band shown in the visible light region is thought to originate from the organic component introduced by the OLD method. The UV-Vis spectrum of citric acid is also plotted in Figure 7. It indicates that the organic component of our $ZnAl_2O_4$ nanoparticle is not simple citric acid or a related material. The FT-IR spectra are also compared in Figure 9 for the $ZnAl_2O_4$ nanoparticles, the sintered reference sample, and citric acid to obtain information about the organic

component of our sample. Figure 9 also indicates that the organic component of our $ZnAl_2O_4$ nanoparticles is not simple citric acid or a related material. The OLD method uses citric acid ($C_6H_8O_7$; $C(OH)(CH_2COOH)_2COOH$) as the organic component and ammonium water as the pH adjuster. Moreover, our hydrothermal process, similar to the typical chemical synthesis, applies high temperature and involves Zn^{2+} ion in the precursor solution. This Zn^{2+} ion has the potential to work as the catalyst to yields amide compound from carboxylic acid in ammonia solution. The FT-IR spectrum of the $ZnAl_2O_4$ nanoparticle shown in Figure 9 can be compared to that of L-glutamine ($C_5H_{10}N_2O_3$; H_2N-CO-(C_2H_4-$CHNH_2$-COOH), which has a similar molecular structure to citric acid with an amide. The characteristic absorption bands originating in the organic component in our $ZnAl_2O_4$ nanoparticles are observed around 1000 ~ 1100 cm^{-1}, 1500 ~ 1700 cm^{-1}, and 2500 ~ 3700 cm^{-1}. Then, the band around 2500 ~ 3700 cm^{-1} is considered a typical

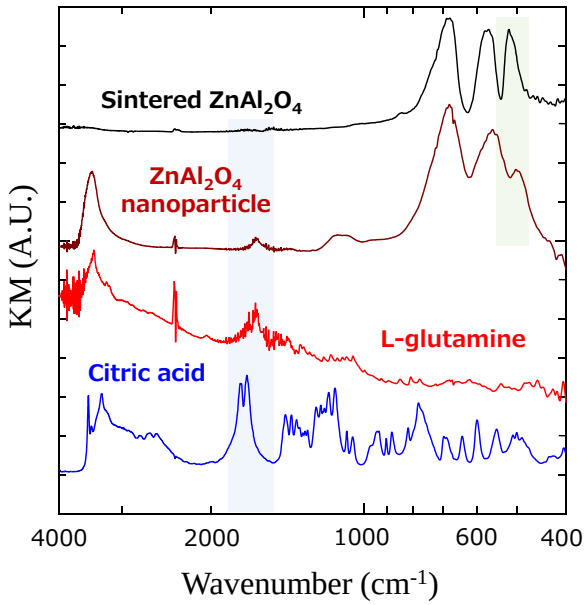

Fig. 9 FT-IR spectrum of $ZnAl_2O_4$ nanoparticle synthesized at 250 °C for 20 hours from the precursor with w = 2.00 and pH ≈ 7. Data are compared with thr FT-IR spectra of sintered $ZnAl_2O_4$ powder heated at 1300 °C, of L-glutamine, and of citric acid.

one originating in the stretching mode of O-H including absorbed H_2O. On the other hand, we cannot assign the band around 1000 ~ 1100 cm^{-1}, unfortunately. However, the peak position of the band around 1500 ~ 1700 cm^{-1} (the blue area in Figure 9) is apparently similar to that of L-glutamine rather than to that of citric acid. This is important, since it is a typical difference in the stretching mode of C=O between carboxylic acid (COOH) and amide ($CO-NH_2$). This result impressed upon us that the citric acid added as the organic component in the OLD method reacts with the ammonium ion of the pH adjuster and works as the surfactant to control the size of the product $ZnAl_2O_4$ nanoparticles. Unfortunately, determination of the molecular structure of this organic component exceeds the focus of this study. However, this result is quite interesting from the viewpoint of the material design for organic-inorganic hybrid nano-materials.

Finally, we comment on the crystal structure of the $ZnAl_2O_4$ nanoparticles produced by hydrothermal synthesis via the OLD method. Figures 1 and 2 show that the 400 peak of the XRD pattern is higher than the 331 peak for all our $ZnAl_2O_4$ nanoparticles. This is expected trend for $ZnAl_2O_4$ having large amount of site exchange phenomenon between Zn^{2+} at tetrahedral site and Al^{3+} at octahedral site within the spinel structure [22]. This trend can also be identified from the FT-IR spectra shown in Figure 9. In the FT-IR spectrum, the site exchange phenomenon of spinel aluminates decrease the intensity of the absorption band around 480 ~ 540 cm^{-1} (the green area in Figure 9) [23,31]. Figure 9 clearly shows this trend. In spinel materials, the site exchange phenomenon is difficult to prevent, but $ZnAl_2O_4$ stands out as an exceptional phase with a remarkably low occurrence (less than 1%) of such exchanges. This understanding is derived

from investigations conducted using samples fabricated through solid-state reaction methods. Thus, fabrication of $ZnAl_2O_4$ with a significant amount of site exchange would be practically impossible through a solid-state reaction route. This study produced it easily through a chemical synthesis route. The site exchange phenomenon is considered one approach to enhance catalytic performance in the case of transition metal aluminates expressed as MAl_2O_4 (*M*: transition metal), since it increases the amount of Al^{3+} in tetrahedral coordination [32,33]. That is, the results of this study are interesting from the perspective of applying metal aluminates as catalysts in various applications.

Summary

$ZnAl_2O_4$ has been actively investigated in some application fields, but a direct bottom-up synthesis route from a liquid precursor solution has not been proposed until now. This study investigated a hydrothermal technique for synthesizing $ZnAl_2O_4$ and proposed the OLD method as a novel synthesis route using a transparent liquid precursor solution. The advantages of the OLD method are that it enables the direct bottom-up synthesis of $ZnAl_2O_4$ and that it is usable across a wide pH range (3.0 ~ 11). These advantages are important for discussing the application of nanoparticles synthesized by hydrothermal technique. For example, if we apply the OLD method, we will be able to synthesize $ZnAl_2O_4$ continuously by applying the flow-type hydrothermal synthesis system [34,35].

Synthesized $ZnAl_2O_4$ was determined to be a single phase based on XRD analysis, even for the sample synthesized over a period of 2 hours. The product $ZnAl_2O_4$ is thought to be in the nanoparticle form, and the particle size was increased by elongation of the heating time. However, the growth rate of the $ZnAl_2O_4$ nanoparticle was not high in the case of hydrothermal synthesis via our OLD method. The average particle size was basically smaller than 10 nm even though the sample was synthesized for 20 hours. This small size suggested the potential for inducing the quantum size effect. In fact, evaluation of UV-Vis spectra suggested the appearance of this effect, and the absorption energy of the bandgap seemed to increase. We attribute the slow growth rate to the existence of organic components in the $ZnAl_2O_4$ nanoparticle. The origin of the components is the organic acid of the OLD method, and it is speculated to work as the surfactant at the phase formation process. The present findings are highly intriguing from the perspective of application studies involving nanoparticles and the design of organic-inorganic hybrid nanomaterials.

On the other hand, ICP-OES measurement reveals the importance of a long heating time (over 1000 minutes) to obtain $ZnAl_2O_4$ without cation deficiency (i.e., Zn : Al = 1 : 2). Additionally, the structural analysis conducted using XRD and FT-IR results reveals that the $ZnAl_2O_4$ nanoparticles synthesized through the hydrothermal technique using the OLD method exhibit a substantial occurrence of site exchange between Zn^{2+} and Al^{3+} within the spinel structure. These results provide crucial data for the future studies of $ZnAl_2O_4$ nanoparticles.

Our OLD method is basically applicable to the synthesis of other spinel oxides. Thus, we believe the OLD method can extensively improve investigations into chemical processing for spinel oxides. Further investigation is required.

Acknowledgements

We acknowledge Dr. H. Isago of the National Institute for Materials Science for his meaningful discussion about the chemical synthesis of complex materials. Compositional analysis using ICP-OES in this study was supported by the NIMS Surface and Bulk Analysis Unit. We are deeply grateful to Dr. Iwanade, Dr. Kato, Dr. Yamaguchi and Ms. M. Hayashi for their technical support. TEM observation was supported by the NIMS Electron Microscopy Unit. Finally, this work was partially supported by a KAKENHI Grant-in-Aid for Challenging Exploratory Research (16K13999).

References

[1] Sampath SK, Kanhere DG, Pandey R (1999) Electronic structure of spinel oxides: zinc aluminate and zinc gallate. J Phys Cond Matter 11: 3635-3644. doi: 10.1088/0953-8984/11/18/301

[2] Dixit H, Tandon N, Cottenier S, Saniz R, Lamoen D, Partoens B Saeybroeck VV, Waroquier M (2011) Electronic structure and band gap of zinc spinel oxides beyond LDA: $ZnAl_2O_4$, $ZnGa_2O_4$ and $ZnIn_2O_4$. New J Phys 13: 063002. doi: 10.1088/1367-2630/13/6/063002

[3] Matsui H, Xu CN, Liu Y, Tateyama H (2004) Origin of mechanoluminescence from Mn-activated $ZnAl_2O_4$: Triboelectricity-induced electroluminescence. Phys Rev B 69:235109. doi: 10.1103/PhysRevB.69.235109

[4] Rojas-Hernandez RE, Rubio-Marcos F, Romet I, Campo Ade, Gorni G, Hussainova I, Fernandez JF, Nagirnyi V (2022) Deep-Ultraviolet Emitter: Rare-Earth-Free $ZnAl_2O_4$ Nanofibers via a Simple Wet Chemical Route. Inorg Chem 61, 11886-11896. doi: 10.1021/acs.inorgchem.2c01646

[5] Bae CH, Lim KS, Babu P (2018) Precipitation of Eu^{3+} - Yb^{3+} Codoped $ZnAl_2O_4$ Nanocrystals on Glass Surface by CO_2 Laser Irradiation. Currnet Opt Phot 2, 79-84. doi: 10.3807/COPP.2018.2.1.079

[6] Nakane T, Naka T, Nakayama M, Uchikoshi T (2022) Humidity Sensitivity of Chemically Synthesized $ZnAl_2O_4$/Al. Sensors 22, 6194-6206. doi: 10.3390/s22166194

[7] Cornu L, Gaudon M, Jubera V (2013) $ZnAl_2O_4$ as a potential sensor: variation of luminescence with thermal history. J Mater Chem C 1: 5419-5428. doi: 10.1039/c3tc30964a

[8] Ishii S, Nakane T, Uchida S, Yoshida M, Naka T (2018) Influence of pH tuning at the precursor preparation process on the structural characteristics and catalytic performance of hydrothermally synthesized $ZnAl_2O_4$ nanoparticles. J Asian Ceram Soc 6:7-12. doi: 10.1080/21870764.2018.1439692

[9] Galetti AE, Gomez MF, Arrua LA, Abello MC (2011) Ethanol steam reforming over Ni/$ZnAl_2O_4$-CeO_2. Influence of calcination atmosphere and nature of catalytic precursor. Appl Catal A: Gen 408: 78-86. doi 10.1016/j.apcata.2011.09.006

[10] Zawadzki M, Staszak W, López-Suárez FE, Illán-Gómez MJ, Bueno-López A (2009) Preparation, characterization and catalytic performance for soot oxidation of copper-containing $ZnAl_2O_4$ spinels. J Appl Catal A: Gen 371: 92-98. doi 10.1016/j.apcata.2009.09.035

[11] Staszak W, Zawadzki M and Okal J (2010) Solvothermal synthesis and characterization of nanosized zinc aluminate spinel used in *iso*-butene combustion. J Alloys Compd 492: 500-507. doi 10.1016/j.jallcom.2009.11.151

[12] Stringhini FM, Mazutti MA, Dotto GL, Jahn SL, Cancelier A, Chiavone-filho O, Foletto EL (2015) Photocatalytic activity of $ZnAl_2O_4$ spinel for procion red degradation under UV irradiation. Lat Am app res 45: 51-55 10.52292/j.laar.2015.371

[13] Battison S, Rigo C, Severo EdaC, Mazutti MA, Kuhn RC, Gündel A, Foletto EL (2014) Synthesis of Zinc Aluminate ($ZnAl_2O_4$) Spinel and Its Application as Photocatalyst. Mater Res 17: 734-738 10.1590/S1516-14392014005000073

[14] Tian Q, Fang G, Ding L, Ran M, Zhang H, Pan A, Shen K, Deng Y (2020) $ZnAl_2O_4/Bi_2MoO_6$ heterostructures with enhanced photocatalytic activity for the treatment of organic pollutants and eucalyptus chemimechanical pulp wastewater. Mater Chem Phys 241: 122299. doi 10.1016/j.matchemphys.2019.122299

[15] Li X, Zhu Z, Zhao Q, Wang L (2011) Photocatalytic degradation of gaseous toluene over $ZnAl_2O_4$ prepared by different methods: A comparative study. J Haz Mater 186: 2089-2096. doi

10.1016/j.jhazmat.2010.12.111

[16] Kumari V, Bhaumik A (2015) Mesoporous $ZnAl_2O_4$: an efficient adsorbent for the removal of arsenic from contaminated water. Dalton Trans 44: 11843-11851. doi 10.1039/C5DT01333J

[17] Miron I, Enache C, Dabici A, Grozescu I (2012) Characterization and luminescence properties of $ZnAl_2O_4:Tb^{3+}$ (2.5%) phosphor. J Optoelect Adv Mater 14: 820-825.

[18] Sun G, Sun G, Zhong M, Wang S, Zu X, Xiang X (2016) Coordination Mechanism, Characterization, and Photoluminescence Properties of Spinel $ZnAl_2O_4$ Nanoparticles Prepared by a Modified Polyacrylamide Gel Route. Russian J Phys Chem 90: 691-699. doi 10.1134/S0036024416030146

[19] Pechini MP, US Patent No. 3.330.697 (1967)

[20] Strachowski T, Grzanka E, Mizaracki J, Chlanda A, Baran M, Małek M, Niedziałek M (2022) Microwave-Assisted Hydrothermal Synthesis of Zinc-Aluminum Spinel $ZnAl_2O_4$. Materials 15: 245-256. doi 10.3390/ma15010245

[21] Foletto EL, Battiston S, Simões JM, Bassaco MM, Pereira LSF, Flores ÉMdeM, Müller EI (2012) Synthesis of $ZnAl_2O_4$ nanoparticles by different routes and the effect of its pore size on the photocatalytic process. Microporous and Mesoporous Mater 163: 29-33. doi 10.1016/j.micromeso.2012.06.039

[22] Ishii S, Nakane T, Furusawa T, Naka T (2016) Synthesis of single-phase $ZnAl_2O_4$ nanoparticles via a wet chemical approach and evaluation of crystal structure characteristics. Cryst Res Technol 51:324–

332. doi 10.1002/crat.201500297

[23] Nakane T, Naka T, Sato K, Taguchi M, Nakayama M, Mitsui T, Matsushita A, Chikyow T (2015) Spectroscopic and crystallographic anomalies of $(Co_{1-x}Zn_x)Al_2O_4$ spinel oxide. Dalton Trans 44: 997-1008. doi 10.1039/C4DT01599A

[24] Scherrer P (1918) Bestimmung der Größe und der inneren Struktur von Kolloidteilchen mittels Röntgenstrahlen. Nachrichten von der Gesellschaft der Wissenschaften zu Göttingen Mathematisch-Physikalische Klasse 26: 98-100

[25] Patterson AL (1939) The Scherrer Formula for X-Ray Particle Size Determination. Phys Rev 56; 978-981. doi: 10.1103/PhysRev.56.978

[26] Kubelka P, Munk F (1931) Ein Beitrag zur Optik der Farbanstriche. Zeit für Tech. Physik 12: 593–601.

[27] Segall MD, Lindan PJD, Probert MJ, Pickard CJ, Hasnip PJ, Clark SJ, Payne MC (2002) First-principles simula-tion: ideas, illustrations and the CASTEP code. J Phys Cond Matter 14: 2717–2744. doi: 10.1088/0953-8984/14/11/301

[28] Payne MC, Teter MP, Allan DC, Arias TA, Joanno-poulos JD (1992) Iterative minimization techniques for abinitio total-energy calculations — molecular-dynamics and conjugate gradients. Rev Mod Phys 64: 1045–10. doi: 10.1103/RevModPhys.64.1045

[29] Rietveld HM (1969) A profile refinement method for nuclear and magnetic structures. J Appl Cryst 2:65-71. doi: 10.1107/S0021889869006558

[30] Izumi F, Momma K (2007) Three-dimensional visualization in powder diffraction. Sol Stat Phenom 130:15-20. doi: 10.4028/www.scientific.net/SSP.130.15

[31] Nakane T, Ishii S, Naka T, Uchikoshi T (2023) Influence of Fabrication Conditions on the Structural Characteristics and the Magnetic Properties of $FeAl_2O_4$. J Am Cerm Soc 106: 2317-2325. doi: 10.1111/jace.18915

[32] Knözinger H, Ratnasamy, P (1978) Catalytic Aluminas: Surface Models and Characterization of Surface Sites. Catal Rev 17;31-70. doi: 10.1080/03602457808080878

[33] Zecchina A, Coluccia S, Morterra C (1985) Infrared Sectra of Molecules Adsorbed on Oxide surfaces. Appl Spectrosc Rev 21;259-310. doi: 10.1080/05704928508060432

[34] Adschiri T, Kanazawa K, Arai K (1992), J. Am. Ceram. Soc. 75: 1019-1022. doi: 10.1111/j.1151-2916.1992.tb04179.x

[35] Adschiri T, Kanazawa K, Arai K (1992), J. Am. Ceram. Soc. 75: 2615-1022. doi: 10.1111/j.1151-2916.1992.tb05625.x